NJC

Accepted Manuscript

This is an *Accepted Manuscript*, which has been through the Royal Society of Chemistry peer review process and has been accepted for publication.

Accepted Manuscripts are published online shortly after acceptance, before technical editing, formatting and proof reading. Using this free service, authors can make their results available to the community, in citable form, before we publish the edited article. We will replace this *Accepted Manuscript* with the edited and formatted *Advance Article* as soon as it is available.

You can find more information about *Accepted Manuscripts* in the Information for Authors.

Please note that technical editing may introduce minor changes to the text and/or graphics, which may alter content. The journal's standard Terms & Conditions and the Ethical guidelines still apply. In no event shall the Royal Society of Chemistry be held responsible for any errors or omissions in this *Accepted Manuscript* or any consequences arising from the use of any information it contains.

ROYAL SOCIETY OF CHEMISTRY

www.rsc.org/njc

Journal Name

ARTICLE

Boron, Nitrogen and Phosphorous Ternary Doped Graphene Aerogel with Hierarchically Porous Structures as Highly Efficient Electrocatalysts for Oxygen Reduction Reaction†

Received 00th January 20xx,
Accepted 00th January 20xx

DOI: 10.1039/x0xx00000x

www.rsc.org/

Hualin Lin,[a]‡ Lei Chu,[a]‡ Xinjing Wang,[a] Zhaoquan Yao,[c] Fan Liu,[a] Yani Ai,[a] Xiaodong Zhuang*[b] and Sheng Han*[a]

Heteroatom doped porous carbons have shown great potential as metal-free catalysts for electrochemical catalyzed oxygen reduction reaction (ORR). Most of previous work have been focused on preparation of single and dual heteroatom doped porous carbons for ORR. In this work, we developed a new two-step method for preparation of boron, nitrogen and phosphorus (B, N, P) ternary doped hierarchically porous graphene aerogels by using boron phosphate as both B and P precursor and ammonia as N dopant. As-produced ternary-doped graphene aerogels exhibited promising ORR performance (mainly 4e$^-$ mechanism, J_k: -4.6 mA cm^{-2}) in alkaline medium in comparsion with commercial available precious metal based Pt/C catalyst. As-prepared B/N/P ternary doped hierarchically porous graphene aerogels can serve as the next generation of metal-free catalysts and alternatives of precious metal catalysts for oxygen reduction reaction and fuel cells.

Introduction

Oxygen reduction reaction (ORR) plays a significant role in many energy storage and conversion devices, for instance, fuel cells and metal-air batteries. [1-4] Traditional precious metal platinum (Pt) is one of the widest used and effective catalysts for ORR.[5, 6] However, the poor durability, toxic fuel cell condition, high cost and scarcity of Pt-based seriously limited its large-scale commercial application for fuel cells.[6, 7] Thus, searching for novel metal-free catalysts with low cost and comparable catalytic activities to Pt catalysts became one of the most emergency issues for oxygen reduction reaction and fuel cells.

Carbon-based materials which have low price, large surface area, promising electrochemical properties and good stability in strong acidic and basic media are regarded as good substitutes of Pt-based catalysts.[8-10] As is known, graphene is one of the best carbon materials for designing metal-free electrocatalysts. However, graphene oxide, one of the widest graphene derivatives with good dispersibility in water, tends to restack and results in surface area decreasing.[11] In order to overcome this, one of the widest and effective method is through heteroatom-doping into graphene, in addition, this approach can create active sites for improving catalysis performance.[12-15] To date, most previous efforts have been devoted to investigating single and dual heteroatom-doped graphenes to improve their catalytic activities. Liu [16] and Su [17] synthesized P-doped and N/S co-doped carbon catalysts, respectively. The ORR peak potential and the kinetic-limiting current density of the former catalyst are -0.31 V and 3.27 mA cm^{-2}, while the latter catalyst shows -0.36 V and 3.9 mA cm^{-2}, respectively. Unfortunately, ternary-doped graphene is still rarely reported so far.

In this work, boron, nitrogen and phosphorus ternary doped graphene aerogels (BNPGAs) were synthesized via a facile two-step method: 1) graphene oxide based hydrothermal process in presence of boron phosphate acting as boron and phosphorous precursors, and 2) ammonia activation process at high temperature. In the second step, ammonia not only acts as N dopant but also acts as micropore-maker. As-prepared ternary doped graphene aerogels show hierarchically porous structures and high specific surface areas up to 216 m^{2}g^{-1}. Acting as electrochemical catalysts, BNPGAs show promising performance for oxygen reduction reaction in alkaline medium in comparison with commercial available Pt/C.

Experimental

Preparation of GO and boron, nitrogen, phosphorus ternary doped graphene aerogels (BNPGAs)

[a] *School of Chemical and Environmental Engineering, Shanghai Institute of Technology, Haiquan Road 100, 201418, Shanghai, P. R. China*
Email: hansheng654321@sina.com
[b] *School of Chemistry and Chemical Engineering, Shanghai Jiao Tong University, Dongchuan Road 800, 200240, Shanghai, P. R. China.*
Email: zhuang@sjtu.edu.cn
[c] *School of Aeronautics and Astronautics, Shanghai Jiao Tong University,Dongchuan Road 800, 200240, Shanghai, P. R. China.*
†Electronic Supplementary Information (ESI) available: see DOI: 10.1039/ x0xx000 00x
‡These authors contributed equally to this work.

All chemicals were purchased from Aldrich and used as received, unless otherwise noted. GO was prepared from natural flake graphite by a modified Hummers method according to the literature.[18] Briefly，5 g flake graphite, 2.5 g sodium nitrate and 115 ml concentrated sulfuric acid was successively added into 1 L beaker which placed in approximately 0 °C ice-water bath with vigorous agitation，afterwards，15 g potassium permanganate was added to the suspension at a slow rate to ensure that the temperature of the suspension lower than 30 °C. After removing the ice-water bath and keep the suspension at 30-40 °C for 30 min，the colours of the mixture gradually became brownish grey. 230 ml deionized water was slowly added into the brownish grey mixture subsequently. The colour of the diluted suspension turned to brown and 15 min later, the suspension was further diluted with 700 mL deionized water and treated with 3% hydrogen peroxide to reduce the residual permanganate as well as the manganese dioxide. The colour of the suspension turned to bright yellow. The suspension was further centrifuged and dialyzed to remove the acid and residual metal ions respectively to produce graphene oxide water suspension.

The boron/phosphorus co-doped graphene aerogel (BPGA) was synthesized via one-step hydrothermal method using boron phosphate (BPO_4) as both boron and phosphorous precursors. Typically, 0.15 g BPO_4, 15 ml deionized water and 30 ml GO (5 mg ml^{-1}) were heated to 80 °C and stirred for 10 min before adding into autoclave. The mixture was then heated to 180 °C for 12 h. After freeze-drying, B/P co-doped graphene aerogel (BPGA) was produced as black monolith.

The as-prepared BPGA was placed in tube furnace and heated to 1000 °C (or 900, 800 °C) for 2h under nitrogen atmosphere. As produced B/P co-doped porous carbon are denoted as BPGA-X (X=1000, 900 and 800) respectively. Then BPGA-X were further activated under NH_3 atmosphere for Y (Y=5, 10, 15) min at X °C. The activated aerogel are denoted as BNPGA-X-Y.

Structure and Morphology Characterizations

Scanning Electron Microscope (SEM) measurements of the samples were performed on S-3400N scanning electron microscope. Transmission Electron microscopy (TEM) characterizations were conducted using a JEM-2100 (JEOL Ltd., Japan) with an accelerating voltage of 200 KV. X-ray diffraction (XRD) was measured by using an X'Pert PW3040/60 diffractometer with Cu Kα radiation. Raman measurements were recorded on an Invia/Reflrx Laser Micro-Raman spectroscope (Renishaw, England) with excitation laser beam wavelength of 532 nm. The powders of materials were placed on clean glass substrates that were used for the Raman measurement. X-ray photoelectron spectroscopy (XPS) experiments were carried out on AXIS Ultra DLD system from Kratos with Al Kα radiation as X-ray source for radiation. The Brunauer–Emmett–Teller (BET) specific surface area was measured on Autosorb-iQ surface area and porosimetry analyzer (Quantachrome Instruments, USA) based on N_2 adsorption.

Electrochemical measurements

The working electrode was prepared by loading a catalyst sample film of 0.60 mg cm^{-2} onto a glass carbon electrode.[19] First, the ink was prepared by dispersing 10 mg of catalyst (BPGA, BPGA-X and BPGA-X-Y) in 500 μL of 1 wt % Nafion ethanol solution, and then sonicating for at least 30 min to form a homogeneous dispersion. Next, 6 μL of the catalyst ink was loaded onto a glassy carbon electrode with a diameter of 5 mm (0.6 mg cm^{-2}). Pt/C ink was prepared by dispersing 4 mg of Pt/C (20 wt% Pt) in 1 mL of ethanol with 35 μL of 5 wt% Nafion solution (40 wt% of Nafion to catalyst ratio), and then 5 μL of Pt/C ink was loaded onto a glassy carbon electrode. The ink was dried slowly in air, and the drying condition was adjusted by trial and error until a uniform catalyst distribution across the electrode surface was obtained.

Electrochemical measurements of cyclic voltammetry (CV), rotating disk electrode (RDE), rotating ring-disk electrode (RRDE) and Chronoamperometric (CA) were performed by a basic bipotentiostat (Pine Research Instrumentation, USA) with a three-electrode cell system. A rotating glass carbon disk and platinum ring electrode (Pine Research Instrumentation, USA) after loading the electrocatalysts was used as the working electrode, an Ag/AgCl (KCl, 3 M) electrode as the reference electrode, and a Pt wire as the counter electrode. The electrochemical experiments were conducted in O_2 saturated 0.1 M KOH electrolyte for the oxygen reduction reaction. The potential range was cyclically scanned between -1.0 and +0 V at a scan rate of 100 mV s^{-1} at the room temperature after purging O_2 gas for 30 min. RRDE were conducted in O_2-saturated 0.1 M KOH electrolyte with a rotation speed of 1600 rpm. The disk electrode was scanned cathodically at a rate of 5 mV s^{-1} and the ring potential was constant at 0.5 V versus Ag/AgCl. RDE measurements were conducted at different rotating speeds from 225 to 2500 rpm in an O_2 saturated 0.1 M KOH solution at 10 mV s^{-1}

The transferred electron number (n) per oxygen molecule in the ORR process at electrode can be calculated by the Koutechy–Levich (K–L) equations (1-3):

$$\frac{1}{J} = \frac{1}{J_L} + \frac{1}{J_K} = \frac{1}{\beta\omega^{1/2}} + \frac{1}{J_K} \quad (1)$$

$$\mathrm{B} = 0.62\mathrm{nF}C_0(D_0)^{2/3}\nu^{-1/6} \quad (2)$$

$$J_K = nFkC_0 \quad (3)$$

in which J is the measured current density, J_K and J_L are the kinetic and diffusion-limiting current densities, respectively, μ is the angular velocity of the rotating electrode (ω= 2πN, where N is the linear rotation speed), F is the Faraday constant (F = 96485 C mol^{-1}), C_0 is the concentration of O_2, D_0 is the diffusion coefficient of O_2, v is the kinematic viscosity of the electrolyte, and k is the electron transfer rate constant. Since the electrolyte is O_2-saturated 0.1 M KOH, C_0, D_0, and *v* are constants: 1.2×10^{-3} M, 1.9×10^{-5} cm^2 s^{-1}, and 0.01 cm^2 s^{-1}, respectively.

Based on the RRDE result, the HO_2^- (%) and the electron transfer number (n) value were calculated based on the RRDE result by the following equations:

$$n = \frac{4I_{Disk}}{I_{Disk}+\frac{I_{Ring}}{N}} \quad (4)$$

$$\%(HO_2^-) = \frac{200\times\frac{I_{Ring}}{N}}{I_{Disk}+\frac{I_{Disk}}{N}} \quad (5)$$

Where I_{disk} is the disk current, I_{ring} is the ring current, and N is current collection efficiency of the Pt ring, which was provided as 0.37 by the manufacturer. A glassy carbon electrode with a diameter of 5.61 mm was used in this experiment.

Results and discussion

The overall synthetic process of boron, nitrogen and phosphorous ternary doped graphene aerogels (BNPGAs) is illustrated in Scheme 1. First, an aqueous dispersion of GO in the presence of boron phosphate was ultrasonicated to form a homogeneous suspension. Then, the black 3D sponge-like B/P co-doped graphene aerogel (BPGA) was constructed through hydrothermal treatment at 180°C for 12 h. Finally, the target B, N, P ternary doped graphene aerogels BNPGA-X-Y were obtained by carbonization of BPGA at X (X=800, 900 and 1000) °C under N_2 atmosphere for 2 h and following activation by ammonia gas for Y (Y=5, 10 and 15) min. In this strategy, boron phosphate acts as both boron and phosphorous precursors, while ammonia acts as both nitrogen precursor and micropore (<2 nm) maker. As is known, graphene aerogel is one kind of porous materials with large amount of macropores (>50 nm). Therefore, this easy strategy not only provide a new method for preparation of ternary doped graphene aerogel, but also provide a new way to hierarchical porous graphene aerogels.

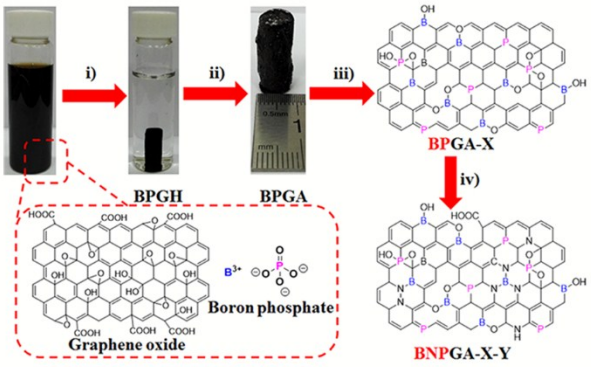

Scheme 1 Schematic illustration of preparation of boron, nitrogen and phosphorus doped graphene aerogels (BNPGAs). i) hydrothermal process, 180 °C, 12h; ii) freeze drying; iii) nitrogen atmosphere, X=800, 900 or 1000°C, 2h; iv) ammonia atmosphere, Y=5, 10 or 15 min.

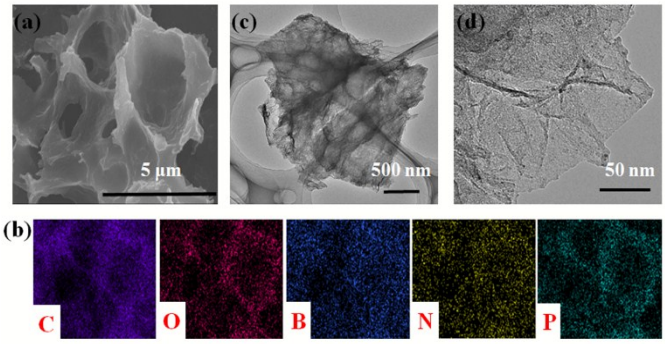

Fig. 1 (a) SEM image and (b) the elemental mapping image of BNPGA-1000-15; (c), (d) TEM images of BNPGA-1000-15.

SEM and TEM were used to reveal the morphology and microstructures of BNPGAs. Due to morphology similarity, BNPGA-1000-15 will be discussed as the typical example unless specified otherwise. The SEM image of BNPGA-1000-15 (Fig.1a) clearly show large pore structures. The sizes of the pores connected by graphene layers ranged from several to dozens of micrometers. The uniform distribution of carbon, oxygen, boron, nitrogen and phosphorous in the 3D porous carbon for BNPGA-1000-15 was observed by SEM elemental mapping over a large region (Fig. 1b). As shown in Figure 1c, the low- magnification TEM image of BNPGA-1000-15 further demonstrates the nanosheet morphology of graphene component. The bright and dark districts were observed from the high-magnification TEM image of BNPGA-1000-15 (Fig. 1d) indicating possible porous structure on graphene surfaces.

Nitrogen physisorption analysis was performed to investigate further the porous features of the as-prepared aerogels (Fig. 2 and S1). As shown in Fig. 2a, the isotherms of the BNPGA-1000-15 show a type IV patterns with pronounced adsorption for mesoporous materials. The specific Brunauer–Emmett–Teller surface area (S_{BET}) and Langmuir surface area (S_{Lang}) of BNPGA-1000-15 were recorded at 216 and 373 m^2g^{-1}, respectively, which were higher than those of BPGAs without ammonia activation (Table 1). Most importantly, the pore size distribution of BNPGA-1000-15 calculated by non-linear density functional theory (NL-DFT) method indicates both microporous pore (1.6 nm) and mesoporous pores (2.7 and 3.9 nm). Taking into account of the large pore observed from SEM image, as-prepared BNPGAs are hierarchically porous graphene possessing micro-, meso- and macropores. However, mainly mesopores can be found for BPGAs (Table 1 and Fig. S1). This result indicates that ammonia activation at high temperature can significantly increase surface area by creating micropores. Moreover, different ammonia activation time of BNPGA-1000 was also carried out. Interestingly, the specific surface area of BNPGA-1000-10 shows the largest BET surface area of 372 m^2g^{-1}.

XPS was carried out to elucidate the valence states of the individual elements of BNPGAs. The typical survey C1s, B1s, P2p and N1s spectra for BNPGA-1000-15 are illustrated in Fig. 3a. The C, N, O, B, N, and P signals can be easily found in the survey spectrum. The doped B and P atoms originated from boron phosphate decomposition. As shown in Fig. 3b, the B1s peaks at 192, 190.5 and 189.2 eV can be attributed to the BN_3

(or B-C-O), sp^2-B-N, and B-C-N bonds, respectively.[20, 21, 22] The B1s XPS spectrum of BPGA (see Fig. S2b) show two types of boron locate at 192 and 193 eV, which can be attributed to B-O and B-C-O respectively. While, the B 1s XPS spectrum of BPGA-1000 (see Fig. S3b) new signals at 191 eV corresponding to BC_3.[20] All these results indicate that high temperature pyrolysis and ammonia activation create B-N bond. The P2p XPS spectra of BPGA, BPGA-1000 and BNPGA-1000-15, (Fig. 3c, S2c and S3c) show the similar P-O binding energy peak at 133.8 eV and P-C binding energy peak at 132.7 eV, [23] enunciating the P-doping feature and unaffected character by ammonia activation. The N 1s XPS spectrum of BNPGA-1000-15 (Fig. 3d) can be deconvoluted into three peaks located at 398.4, 399.8 and 401.3 eV, which can be attributed to pyridinic-N, C-N-B, sp^3-N-C, respectively.[24, 25] According to these results, B, N and P elements have been successfully doped in graphene by a simple two-step method. The XPS spectra of BPGA, BPGA-X (X=800, 900 and 1000) and BPGA-X-Y (Y=15, X=800-1000; X=1000, Y=5-15) were illustrated in Fig. S2-S5.

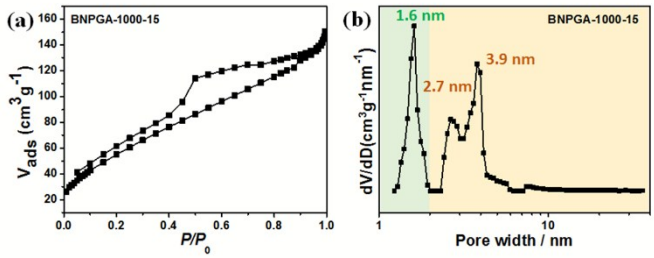

Fig. 2 (a) N_2 sorption-desorption isotherms and (b) the corresponding pore size distribution of BNPGA-1000-15 calculated by NL-DFT method.

To explore their crystalline structures, the as-prepared sponge-like aerogels were characterized via XRD. As shown in Fig. 4a and S6, characteristic peak of BPGA at 2θ=28° disappeared in the XRD patterns of BNPGA-X-15. This results was consistent with the results of the aforementioned B1s XPS spectra of BPGA and BNPGA-1000-15. BNPGA-X-15 and BPGA appear the obvious graphite peak at 2θ=26° and the peak intensity show a slightly increase after pyrolysis at high temperature under NH_3 atmosphere. This result indicates that the crystalline structure of graphene increases after pyrolysis and ammonia activation.[20, 26] Moreover, the XRD patterns of BPGA-X (X=800, 900 and 1000), BNPGA-1000-5 and BNPGA-1000-10 in Fig. S6 shows that the weak boron oxide (B_2O_3) peak are vanished after pyro lysis and ammonia activation.

Table 1 Nitrogen physisorption results for BPGA, BPGA-X and BNPGA-X-Y.

Samples	S_{BET} [a]	S_{Lang} [b]	S_{micro} [c]	v_{tot} [d]	V_{micro} [d]	d_{av} [f]
BPGA	13	48	-	0.02	-	7.63
BPGA-800	49	192	-	0.07	-	5.73
BPGA-900	79	151	-	0.1	-	5.73
BPGA-1000	20	39	-	0.03	-	6.95
BNPGA-800-15	110	187	18	0.15	0.009	5.37
BNPGA-900-15	166	256	46	0.36	0.028	8.72
BNPGA-1000-15	216	373	36	0.23	0.017	4.30
BNPGA-1000-10	372	557	188	0.34	0.097	3.60
BNPGA-1000-5	93	130	47	0.09	0.021	4.21

(a) BET surface area (m^2g^{-1}) and (b) Langmuir surface area (m^2g^{-1}) calculated from the nitrogen adsorption based on the BET and Langmuir methods respectively. (c) Surface area of micropore (m^2g^{-1}). (d) The total pore volume (cm^3g^{-1}) calculated at P/P_0 = 0.99. (e) Pore volume of micropore (cm^3g^{-1}). (f) Average pore diameter (nm).

The Raman spectra of BPGAs and BNPGAs were obtained and shown in Fig. 4b and S7 to confirm the defects and degree of order of graphene. No obvious shifts was observed for the two distinct peaks emerged near at 1350 and 1590 cm^{-1}, which were attributed to the D band and the G band, respectively. The D band is commonly associated with defect sites or disordered sp^2-hybridized carbon atoms of graphite, whereas the G band is observed for all graphitic structures due to the first-order scattering of the E_{2g} mode. The ratio of the D and G band intensities (I_D/I_G) is generally used as measure disorder of carbon materials. Usually, the higher I_D/I_G values means the more defects in the carbon structure. [20, 26, 27, 28] The I_D/I_G value of BNPGA-1000-15 (1.12) was slightly higher than that of BNPGA-900-15 (1.10), BNPGA-800-15 (1.09) and BPGA (0.98), indicating the defects of BNPGAs increases after pyrolysis temperature increases. The I_D/I_G values increased owing to the rich C-B, C-P and C-N bonds and further proved that the heteroatoms (B, P, N) doping feature in graphene.[20] Interestingly, the I_D/I_G values of BPGA-X (X=800, 900 and 1000), BNPGA-1000-5 and BNPGA-1000-10 decreases sequentially (Fig. S7). This indicates that pyrolysis of BPGA with the increased temperature and prolonged ammonia activation time can reduce the defect sites as well as enhanced the degree of sp^2-carbon.

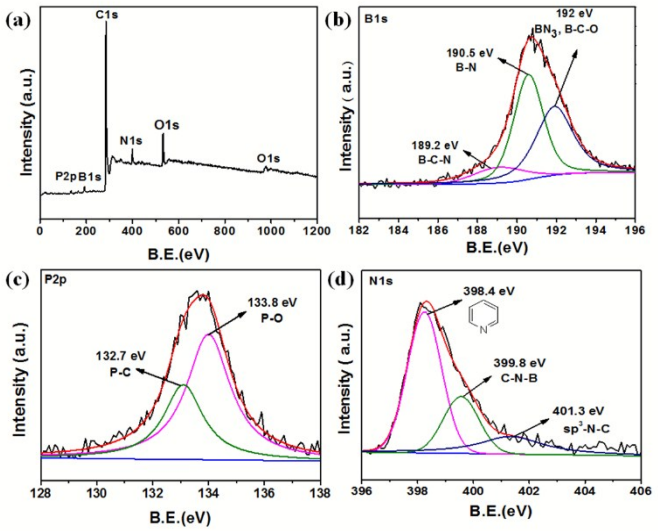

Fig. 3 XPS (a) survey, (b) B1s, (c) P2p and (d) N1s spectra of BNPGA-1000-15.

As is known, the porous structure and the rich heteroatom-involved defects could boost the diffusion of reactants which is favourable to the electrochemical catalysed oxygen reduction reaction (ORR).[29-31] The electrocatalytic activities of as-prepared ternary doped porous graphene aerogel for ORR were carried out under alkaline condition (0.1 M KOH). BPGA, BPGA-X and BNPGA-X-Y were firstly measured by cyclic voltammetry (CV, Fig. 5a, S8 and S9) sweeping in O_2 and N_2-saturated 0.1 M KOH solution. Typically, the cyclic

voltammetry (CV) of BNPGA-1000-15 in O_2 and N_2-saturated 0.1 M KOH was shown in Fig. 5a. It is found that the ORR peak for BNPGA-1000-15 locates at -0.19 V versus Ag/AgCl catalysts which is about 0.08 V more positive than that of BNPGA-900-15 (-0.27 V) and 0.17 V positive than that of BNPGA-800-15 (-0.36 V). Interestingly, BPGA shows no obvious ORR peak possibly due to the poor conductivity. Among all as-prepared BPGAs and BNPGAs, BNPGA-1000-15 exhibited most negative ORR peak indicating possible easiest ORR reaction for BNPGA-1000-15.[29, 32-36] To compare the catalytic activities of BNPGAs with commercial Pt/C, LSV (Fig. 5b, S10) was carried out in O_2-saturated0.1 M KOH solution at a rotation rate of 1600 rpm with a scanning rate of 10 mV S^{-1}.BNPGA-1000--15 shows the lowest onset potential at -0.06 V among BPGAs and BNPGAs and a bit smaller than that of Pt/C (-0.05 V). The limiting current densities (Table 2) for BNPGA-1000-15 and Pt/C were -4.6 mA cm^{-2} and -5.45 mA cm^{-2} at -1.0 V versus Ag/AgCl, respectively. Based on these results, it is clear that BNPGA-1000-15 shows the most positive onset potential and almost the highest limiting current density among as-prepared aerogels indicating a lower operation voltage and lower energy consumption toward ORR [24] than other aerogels.

It is well known that ORR can proceed either by a two-step

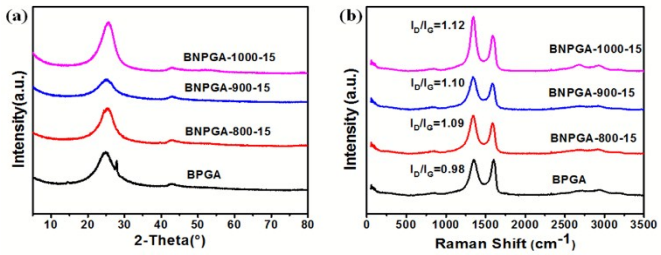

Fig. 4 (a) XRD patterns and (b) Raman spectra of BPGA and BNPGA-X-15 (X=800, 900 and 1000).

two-electron pathway with formation of HO_2^- in alkaline medium as the intermediate species or by a more efficient four-electron process to directly reduce O_2 into OH^- in alkaline medium followed by combining with a proton which derived from the decomposition of pumping hydrogen onto the anode into water.[37]

$O_2 + 2H_2O + 4e^- \rightarrow 4OH^-$ (four-electron process)

$O_2 + H_2O + 2e^- \rightarrow HO_2^- + OH^-$ (two-electron process)

The two-electron pathway decreases the cell potential in polymer electrolyte membrance full cells (PEMFCs) and accelerate the degradation of membrane and catalysts by reacting with H_2O_2. Therefore, the four-electron pathway is desired for practical application.[20, 37]

In order to reveal the electron transfer number (n) for the catalysts, the rotating ring-disk electrode (RRDE) was further carried out. Typically, the RRDE of BNPGA-1000-15 was shown in Fig. 5c. Based on equation 4 and 5, n and hydrogen peroxide percentage can be easily calculated (Fig. 5d).The n for BNPGA-1000-15 was found to be about 3.7 at -1.0 V based on RRDE which is close to that of commercial Pt/C (3.8 at -1.0 V).[38] Linear sweep voltammograms (LSVs) can also be used to determine the n. A series of LSVs of BNPGA-1000-15 were performed with varying rotation speeds from 225 to 2500 rpm in 0.1 M KOH saturated with O_2 (Fig. 5e). Koutecky–Levich (K-L) plots (Fig. 5f) calculated from LSV show a good linear relationship for the BNPGA-1000-15 at different potentials. The n of BNPGA-1000-15 was calculated to be about 3.8 according to the slopes of K-L plots at the potential range from -0.5 V to -0.1 V, indicating a mainly four-electron pathway for ORR.[21] For comparison, LSV curves for BPGA, BPGA-X (X=800, 900 and 1000), BPGA-X-Y (Y=15, X=800, 900; X=1000, Y=5, 10) were also measured. The corresponding K-L plots of for these catalysts also displayed good linearity (Fig. S11-S14). The n values (Table 2) of BPGA, BPGA-X (X=800, 900 and 1000), BPGA-X-Y (Y=15, X=800, 900; X=1000, Y=5, 10) calculated by LSV curves, respectively, which are similar to the results based on RRDE calculation method (Fig. S15).

For the intermediate peroxide species yield, as shown in (Fig. 5d,S15 and Table 2) the lowest percentage of HO_2^- for BNPGA-1000-15 were about 11 % at about -0.2 V versus Ag/AgCl which is slightly higher than that of commercial Pt/C and lower than those of BPGA, BPGA-X, BNPGA-X-15 (X=800, 900) and BNPGA-1000-Y (Y=5, 10). It is noticed that the percentage of HO_2^- for the B/N/P ternary doped catalysts after ammonia activation are obvious less than those of the B/P co-doped catalysts. This result is in good agreement with the result based on calculated n. Thus, we can conclude that B/N/P ternary doping is more favourable for ORR due to more active sites after ammonia activation. To quantitatively judge the ORR performance, the calculated kinetic limiting current (J_k) at -0.6V based on RDE measurement is shown in Fig. 6. The J_k value of BNPGA-1000-15 which is similar to that of Pt/C, is much higher than those of BPGA, BPGA-X, BNPGA-X-15 (X=800, 900) and BNPGA-1000-Y (Y=5, 10). The high J_k value for BNPGA-1000-15 implies the possible synergistic effect between B, N and P heteroatoms and brings enhanced catalytic activity.[38] Moreover, we compared our ternary doped graphene to previous reported single, dual and ternary doped porous carbon materials (Table 3), the more positive ORR peak potential, the larger kinetic limiting current and the better electron transfer number can be identified, indicating that our catalyst prefers to reduce oxygen molecules with $4e^-$ transfer mechanism.

In order to evaluate the durability of the catalysts, the continuous chronoamperometric measurements were performed at -0.3 V versus Ag/AgCl for about 6 h in an O_2-saturated 0.1 M KOH solution compared with commercial Pt/C. According to the above discussed ORR results, typically BNPGA -1000-15 was further tested at a constant voltage of -0.3 V for 20000 s in 0.1 M KOH solution saturated with O_2 at a rotation rate of 1600 rpm (Fig. 7a). Remarkably, the corresponding current–time (i–t) chronoamperometric response of BNPGA-1000-15 exhibited a very slow attenuation after a fast decrease of 5% within the first 200 s, and a high relative current of 88.3 % still persisted after 20000 s. In contrast, Pt/C showed a gradual decrease, with a current loss of approximately 19% measured after 20000 s. This suggests that the durability of BNPGA-1000-15 is superior to that of the commercially available Pt/C catalyst.

Journal Name

ARTICLE

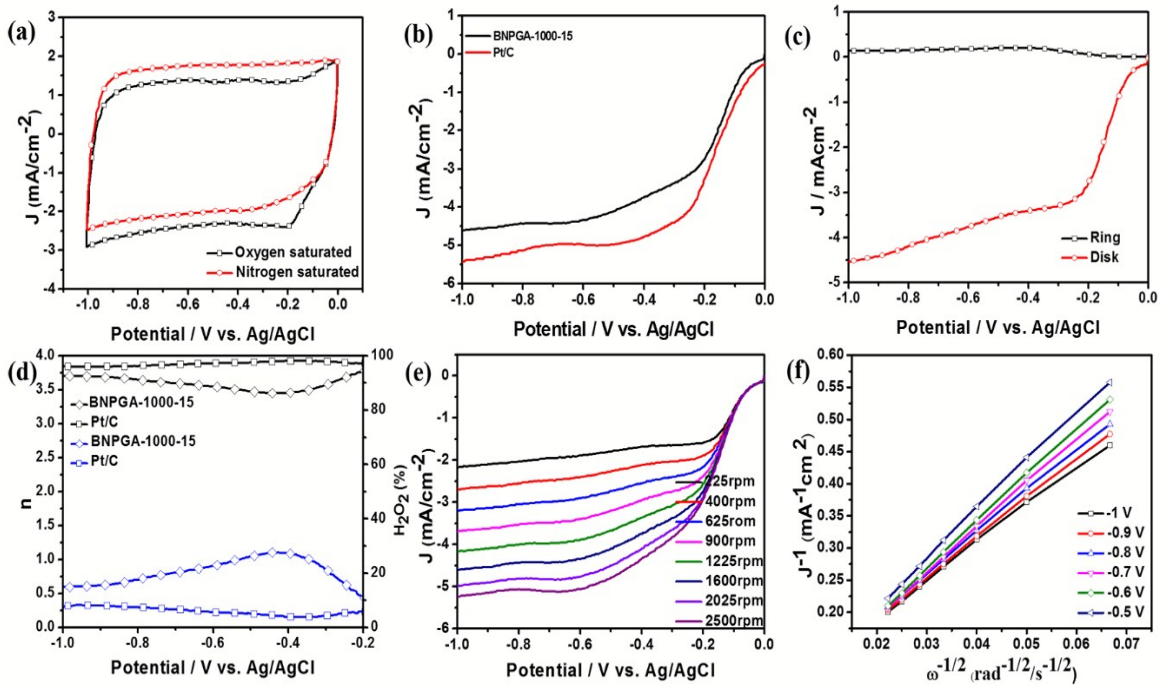

Fig. 5 (a) cyclic volutammograms of BNPGA-100-15 at a scan rate of 100 mV s^{-1} in O_2 and N_2-saturated 0.1M KOH solution. (b) LSVs of BNPGA-1000-15 and commercial Pt/C at a rotation rate of 1600 rpm with a scan rate of 10 mV s^{-1} in O_2- saturated 0.1 M KOH solution. (c) Rotating ring-disk electrode (RRDE) voltammograms of BNPGA-1000-15 with a rotation rate of 1600 rpm at 10 mV s^{-1} in O_2-saturated 0.1 M KOH solution. (d) The calculated electron transfer numbers (n) and percentage of H_2O_2 of BNPGA-1000-15 in comparison with commercial Pt/C. (e) RDE voltammograms of BNPGA-100-15 at different rotating speeds with a scan rate of 10 mV s^{-1} in O_2-saturated 0.1 M KOH solution. (f) Koutecky–Levich plots of BNPGA-1000-15.

Table 2. The ORR catalytic performance of as-prepared materials (*vs.* Ag/AgCl).

Samples	ORR Peak / V	Onset potential / V	J_K/mA cm^{-2}	n	HO_2^-%
BPGA	0	-0.14	-3.97	3.4	29
BPGA-800	-0.27	-0.16	-4.14	3.1	54
BPGA-900	-0.23	-0.18	-4.83	2.7	73
BPGA-1000	-0.24	-0.24	-4.24	2.8	70
BNPGA-800-15	-0.36	-0.21	-3.76	3.2	32
BNPGA-900-15	-0.27	-0.11	-4.01	3.5	12
BNPGA-1000-15	-0.19	-0.06	-4.6	3.7	11
BNPGA-1000-10	-0.27	-0.13	-4.05	3.3	20
BNPGA-1000-5	-0.39	-0.12	-4.27	3.1	39
Pt/C		-0.05	-5.54	3.8	6

Journal Name

ARTICLE

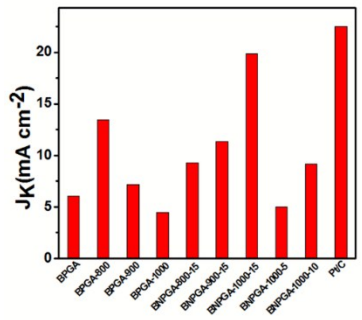

Fig. 6 The calculated kinetic limiting currents (J_k) of BPGA, BPGAs, BNPGAs and commercial Pt/C.

Table 3. ORR catalytic performance of as-developed catalysts in 0.1 M KOH.

Samples	ORR Peak /v	J_k /mA cm^{-2}	n	Ref.
BNPGA-1000-15	-0.19	4.6	3.8	This work
P-doped	-0.22	1.4	3.6	Ref.[39]
P-doped	-0.31	3.3	3.4	Ref.[16]
N/S-doped	-0.36	3.9	3.9	Ref.[17]
N/P/S-doped	-0.38	2.8	3	Ref.[40]

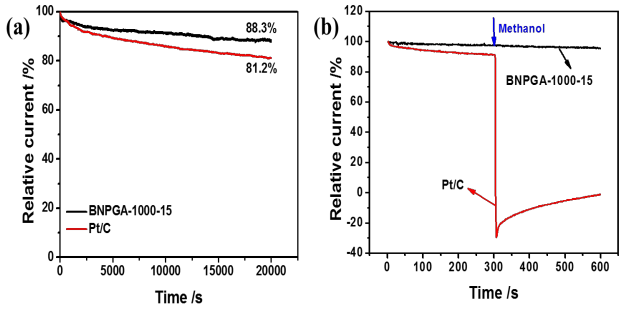

Fig. 7 (a) Current–time (i–t) chronoamperometric response of BNPGA-1000-15 and commercial Pt/C at -0.3 V in O_2-saturated 0.1 M KOH at a rotation rate of 1600 rpm; (b) chronoamperometric responses in O_2-saturated 0.1 M KOH for BNPGA-1000-15 (black line) and Pt/C (red line) electrocatalysts at -0.3 V. The arrow indicates the addition of 2% (v/v) methanol.

To further evaluate the stability, the crossover effect should be considered because fuel molecules such as methanol in the anode sometimes permeate through the polymer membrane to the cathode and seriously affect the performance of the cathode catalysts. Therefore, we further measured the electrocatalytic selectivity of BNPGA-1000-15 and Pt/C against the electro-oxidation of methanol for the ORR, as shown in Fig. 7b. After the addition of 2% (v/v) methanol, the ORR current for BNPGA-1000-15 was almost unchanged, while Pt/C showed a sharp decrease, and even exhibited negative current. Thus, BNPGA-1000-15 indeed has a high selectivity for methanol, and a remarkable ability to avoid crossover effects, superior to the commercially available Pt/C catalyst. This result may be attributed to the synergistic effect of N, B, P containing active sites among the carbon framework. Heteroatom (B, N, P) –doping can break the electro-neutrality of sp^2 carbon in graphene[41] and induce charge redistribution around the heteroatom dopants, which could effectively weaken the O–O bond after chemisorption of oxygen molecules and facilitate the ORR process.[42] Boron and phosphorus tend to donate electrons to carbon, thus creating a partial positive charge on the dopant atoms. On the other hand, nitrogen, which has higher electronegativity than carbon, tends to receive electrons from carbon, thus generating a partial positive charge on the carbon atoms. The formation of partial positive and negative charges can favour the interaction between O_2 and the doped graphene materials.[43] Moreover, the calculated high N/C, B/C, P/C ratio based on XPS result (Table S1) indicates that BNPGA-1000-15 has higher total nitrogen, boron, phosphorus contents than other as-developed materials, which plays a significant role in improving the ORR activity through providing more active sites. [44, 45]

All these results indicate that B, N, P ternary doped graphene aerogels have significant impact on CV peak potential, electron transfer numbers, percentage of HO_2^-, onset potential and limiting current density. The doped heteroatoms (B, N, P) could cause the electronegativity changing of carbon framework (N: 3.04 > C: 2.55 > P: 2.19 > B: 2.04) which synergistically to the ORR activities.[9a, 16a, 20] Beside this, large specific surface area, hierarchically porous structure and nanosheet based continuous 3D carbon framework can supply numerous accessible channels which are favourable for the efficient mass transport and electron conducting for ORR.[46]

Conclusions

In summary, boron, nitrogen and phosphorus ternary doped graphene aerogels (BNPGAs) were successfully prepared via a facile two-step method. Graphene oxide and boron phosphate were used as carbon source and B/P precursors respectively. Ammonia activation not only brings the B/P co-doped graphene aerogel third nitrogen dopant but also creates large amount of micropores and render as-prepared graphene aerogels as hierarchically porous materials with micro-, meso- and macropores inside. Acting as electrochemical catalysts, BNPGAs show promising performance (mainly 4e$^-$ charge transfer mechanism, high kinetic limiting current density up to 19.8 mAcm^{-2}) for oxygen reduction reaction in alkaline medium

in comparison with commercial available Pt/C. All these results indicate that as-prepared B/N/P ternary doped hierarchically porous graphene aerogels can serve as the next generation of metal-free catalysts and alternatives of precious metal catalysts for oxygen reduction reaction and fuel cells.

Acknowledgements

This project was supported by National Natural Science Foundation of China (51403126, 20976105), Shanghai Leading Academic Discipline Project (J51503), Shanghai Association for Science and Technology Achievements Transformation Alliance Program (LM201559), Shanghai Municipal Education Commission boosting project (15cxy39), Science and Technology Commission of Shanghai Municipality Project (14520503200), Shanghai Municipal Education Commission (Plateau Discipline Construction Program), Shanghai Talent Development Funding (201335) .

Notes and references

1. M. Liu, R. Zhang and W. Chen, *Chem. Rev.*, 2014, 114, 5117-5160.
2. A. Ambrosi, C. Chua, A. Bonanni and M. Pumera, *Chem. Rev.*, 2014, 114, 7150-7188.
3. S. Navalon, A. Dhakshinamoorthy, M. Alvaro and H. Garcia, *Chem. Rev.*, 2014, 114, 6179-6212.
4. A. Narita, X. Wang, X. Feng and K. Müllen, *Chem. Soc. Rev.*, 2015, 44, 6616-6643.
5. E. Antolini, *ChemElectroChem*, 2014, 1, 318-328.
6. M. Cao, D. Wu and R. Cao, *ChemCatChem*, 2014, 6, 26-45.
7. B. Xia, H. Wu, N. Li, Y. Yan, X. Lou and X. Wang, *Angew. Chem., Int. Ed.,* 2015, 127, 3868-3872.
8. Y. Zhai, Y. Dou, D. Zhao, P. Fulvio, R. Mayes and S. Dai, *Adv. Mater.*, 2011, 23, 4828-4850.
9. L. Dai, D. Chang, J. Baek and W. Lu, *Small*, 2012, 8, 1130-1166.
10. L. Hao, X. Li and L. Zhi, *Adv. Mater.*, 2013, 25, 3899-3904.
11. L. Wang, Z. Sofer, A. Ambrosi, P. Šimek and M. Pumera, *Electrochem. Commun.*, 2014, 46, 148-151.
12. X. Wang, G. Sun, P. Routh, D. Kim, W. Huang and P. Chen, *Chem. Soc. Rev.*, 2014, 43, 7067-7098.
13. J. Paraknowitsch and A. Thomas, *Energ. Environ. Sci.*, 2013, 6, 2839-2855.
14. J. Liu, P. Song, Z. Ning and W. Xu, *Electrocatalysis*, 2015, 6, 132-147.
15. C. Rao, K. Gopalakrishnan and A. Govindaraj, *Nano Today*, 2014, 9, 324-343.
16. Z. Liu, F. Peng, H. Wang, H. Yu, W. Zheng and X. Wei, *J. Nat. Gas. Chem.*, 2012, 21, 257-264.
17. Y. Su, Y. Zhang, X. Zhuang, S. Li, D. Wu, F. Zhang and X. Feng, *Carbon*, 2013, 62, 296-301.
18. W. Hummers Jr and R. Offeman, *J. Am. Chem. Soc.*, 1958, 80, 1339-1339.
19. Y. Liang, H. Wang, P. Diao, W. Chang, G. Hong, Y. Li, M. Gong, L. Xie, J. Zhou, J. Wang, T. Regier, F. Wei and H. Dai, *J. Am. Chem. Soc.*, 2012, 134, 15849-15857.
20. C. Choi, S. Park and S. Woo, *ACS Nano*, 2012, 6, 7084-7091.
21. S. Zhao, J. Liu, C. Li, W. Ji, M. Yang, H. Huang, Y. Liu and Z. Kang, *ACS Appl. Mater. Inter.*, 2014, 6, 22297-22304.
22. X. Zhuang, D. Gehrig, N. Forler, H. Liang, M. Wagner, M. Hansen, F. Laquai, F. Zhang and X. Feng, *Adv.Mater.*, 2015, 27,3789-3796.
23. D. Yang, D. Bhattacharjya, S. Inamdar, J. Park and J. Yu, *J. Am. Chem. Soc.*, 2012, 134, 16127-16130.
24. J. Wang, Z. Xu, Y. Gong, C. Han, H. Li and Y. Wang, *ChemCatChem*, 2014, 6, 1204-1209.
25. L. Chen, R. Du, J. Zhu, Y. Mao, C. Xue, N. Zhang, Y. Hou, J. Zhang and T. Yi, *Small*, 2015, 11, 1423-1429.
26. C. Zhang, N. Mahmood, H. Yin, F. Liu and Y. Hou, *Adv. Mater.*, 2013, 25, 4932-4937.
27. S. Li, D. Wu, H. Liang, J. Wang, X. Zhuang, Y. Mai, Y. Su and X. Feng, *ChemSusChem*, 2014, 7, 3002-3006.
28. A. Yazdi, H. Fei, R. Ye, G. Wang, J. Tour and U. Sundararaj, *ACS Appl. Mater. Inter.*, 2015, 7, 7786-7794.
29. J. Liang, Y. Jiao, M. Jaroniec and S. Qiao, *Angew. Chem., Int. Ed.*, 2012, 51, 11496-11500.
30. S. Yang, L. Zhi, K. Tang, X. Feng, J. Maier and K. Müllen, *Adv. Funct. Mater.*, 2012, 22, 3634-3640.
31. S. Yang, X. Feng, X. Wang and K. Müllen, *Angew. Chem., Int. Ed.*, 2011, 50, 5339-5343.
32. X. Zhuang, F. Zhang, D. Wu, N. Forler, H. Liang, M. Wagner, D. Gehrig, M. R. Hansen, F. Laquai and X. Feng, *Angew. Chem., Int. Ed.*, 2013, 52, 9668-9672.
33. C. Cao, X. Zhuang, Y. Su, Y. Zhang, F. Zhang, D. Wu and X. Feng, *Polym. Chem.*, 2014, 5, 2057-2064.
34. S. Han, Y. Feng, F. Zhang, C. Yang, Z. Yao, W. Zhao, F. Qiu, L. Yang, Y. Yao and X. Zhuang, *Adv. Funct. Mater.*, 2015, 25, 3899-3906.
35. X. Zhuang, Y. Mai, D. Wu, F. Zhang and X. Feng, *Adv. Mater.*, 2015, 27, 403-427.
36. W. Yang, T. Fellinger and M. Antonietti, *J. Am. Chem. Soc.*, 2010, 133, 206-209.
37. L. Dai, Y. Xue, L. Qu, H. Choi and J. Baek, *Chem. Rev.*, 2015, 115, 4823-4892.
38. Y. Zheng, Y. Jiao, L. Ge, M. Jaroniec and S. Qiao, *Angew. Chem., Int. Ed.*, 2013, 125, 3192-3198.
39. R. Li, Z. Wei, X. Gou and W. Xu, *RSC Adv.*, 2013, 3, 9978-9984.
40. S. Dou, A. Shen, Z. Ma, J. Wu, L. Tao and S. Wang, *J. Electroanal. Chem.*, 2015, 176, 135-151.
41. S. Dou, A. Shen, Z. Ma, J. Wu, L. Tao and S. Wang, *J. Electroanal. Chem.*, 2015, 753, 21-27.
42. J. Zhang and L. Dai, *ACS Catal.*, 2015, 5, 7244-7253.
43. N. Daems, X. Sheng, I. Vankelecom and P. Pescarmona, *J. Mater. Chem. A*, 2014, 2, 4085-4110.
44. J. Sanetuntikul, T. Hang and S. Shanmugam, *Chem. Commun.*, 2014, 50, 9473-9476.
45. G. Jo, J. Sanetuntikul and S. Shanmugam, *RSC Adv.*, 2015, 5, 53637-53643.
46. H. Liang, X. Zhuang, S. Brüller, X. Feng and K. Müllen, *Nat. Commun.*, 2014, 5, 4793.

ToC:

Highly efficient catalysts (mainly $4e^-$ mechanism, J_k: -4.6 mA cm^{-2}) for ORR based on B/N/P ternary-doped graphene aerogels were developed.